Journal of ELECTRONIC MATERIALS, Vol. 39, No. 9, 2010
DOI: 10.1007/s11664-009-1059-x

Thermoelectric Properties as a Function of Electronic Band Structure and Microstructure of Textured Materials

A. JACQUOT,[1,4] N. FARAG,[2] M. JAEGLE,[1] M. BOBETH,[2] J. SCHMIDT,[3] D. EBLING,[1] and H. BÖTTNER[1]

1.—Department of Thermoelectric Systems, Fraunhofer-Institut für Physikalische Messtechnik IPM, Heidenhofstraße 8, 79110 Freiburg, Germany. 2.—Institute for Materials Science and Max Bergmann Center of Biomaterials, Dresden University of Technology, 01062 Dresden, Germany. 3.—Fraunhofer-Institut für Fertigungstechnik und Angewandte Materialforschung IFAM, Institutsteil Dresden, Dresden, Germany. 4.—e-mail: alexandre.jacquot@ipm.fraunhofer.de

A tool has been developed at Fraunhofer-IPM to calculate the transport properties of thermoelectric material by using its band structure described in terms of effective masses and the location of the ellipsoids in reciprocal space. The calculated transport properties are compared with experimental data measured on bismuth telluride, antimony telluride, and bismuth antimony telluride. Polycrystalline specimens have been prepared by spark plasma sintering (Fraunhofer-IFAM). Electron backscattering diffraction analysis of sample cross-sections yields the frequency distribution of grain orientations. This texture information permits the generation of appropriate finite-element models of the polycrystalline microstructure (TU Dresden). By means of the commercial code COMSOL, which allows anisotropic thermoelectric properties to be taken into account, the effective electrical and thermal conductivities as well as the Seebeck coefficient both parallel and perpendicular to the pressing direction have been calculated.

Key words: Thermoelectric, electronic band structure, textured materials, texture, Seebeck, electrical conductivity, thermal conductivity, lattice thermal conductivity, bismuth telluride, antimony telluride, bismuth antimony telluride, effective mass, inertial effective mass, density of states, Boltzmann, COMSOL finite-element method, transport properties, invariance method, Fermi level

INTRODUCTION

In polycrystalline material for which the thermoelectric properties of a single crystal of the same composition are anisotropic, as is the case for sintered materials containing Bi_2Te_3 and/or Sb_2Te_3, the effective thermoelectric properties of the polycrystal are a rather complex function of both grain orientations and the thermoelectric properties in each grain. For polycrystalline material with isotropic grain orientation distribution, the decrease of the figure of merit can be roughly estimated by using analytical formulae, assuming that making a single-crystalline material polycrystalline, for example by pulverization and sintering, does not change the carrier concentration.[1] However, the sintering process is known to introduce defects and to change the carrier concentration and thus the thermoelectric properties significantly. Additionally, sintered materials may exhibit texture.[2]

The objective of this article is to present two methods for determining the thermoelectric properties of sintered materials, both parallel and perpendicular to the pressing direction. The first method is presented for the first time herein and is a rather rough approximation based on a band-structure model of the single crystal which uses the invariance of the trace of a matrix with respect to rotation of the coordinate system to estimate the

(Received July 10, 2009; accepted December 13, 2009; published online February 3, 2010)

properties of the polycrystalline material in one direction if the transport property has been measured in the perpendicular direction. Thus, it is denoted the invariance method in the following. The second method is known as the representative volume element (RVE) method. It is based on the finite-element method (FEM) and allows more accurate calculations of the macroscopic or effective properties of the polycrystalline material, using single-crystal data and the experimentally determined texture. Both methods are explained below.

MODELING OF THE SINGLE CRYSTAL

Exact calculation of the thermoelectric properties of a single crystal is an extremely difficult task. A software suite for performing such calculations should contain two software packages dedicated to the electronic and lattice properties. The first software package should be able to perform at least the calculation of the electronic band structure[3–5] and the relaxation time,[6,7] and be able to use the results to calculate the electrical conductivity and the Seebeck coefficient. The second software package should calculate the lattice dynamics, perhaps also taking into account anharmonic effects, and then use the results to calculate the thermal conductivity.[8]

The present work outlines a rather simpler way of calculating the thermoelectric properties of single-crystalline Bi_2Te_3, Sb_2Te_3, and the solid solution $75\%Sb_2Te_3$-$25\%Bi_2Te_3$. The method is not purely theoretical but also makes use of experimentally determined effective masses found in databases to describe the band structure.[9,10] If the constant-energy surfaces are approximated by ellipsoids, the shape of the ellipsoid is described by one longitudinal (m_3) and two transverse effective masses (m_1, m_2). In the following derivation, the density-of-state effective masses and the inertial effective masses along the crystallographic axes are given as functions of the longitudinal and transversal effective masses of the ellipsoid and as functions of the few parameters that describe the position of the ellipsoids in the first Brillouin zone. Finally, the equations that relate the density-of-states effective masses, the relaxation time, and the Fermi level to the electrical conductivity, the Seebeck coefficient, and the electronic part of the thermal conductivity are derived from the electron gas theory for a single-band model.[11,12]

Effective Masses in Bi_2Te_3, Sb_2Te_3, and $75\%Sb_2Te_3$-$25\%Bi_2Te_3$

The first Brillouin zone of Bi_2Te_3, Sb_2Te_3, and $75\%Sb_2Te_3$-$25\%Bi_2Te_3$ are shown in Fig. 1a. Six ellipsoids that represent constant-energy surfaces are distributed at the center of the square surface at the critical high-symmetry point X. The density-of-states effective mass of a single valley is given by $m^* = (m_1 m_2 m_3)^{1/3}$. The total density-of-states effective mass for the six valleys, which enters the calculation of the Fermi level for a given carrier concentration, is simply obtained by multiplying the density-of-states effective mass of a single valley by $N_V^{2/3} (N_V = 6)$. The calculation of the inertial effective masses along the main axes (K_X'', K_Y'', K_Z'') in the coordinate system of the first Brillouin zone requires a transformation of $[1\hat{/}m]_{\text{single}} = \hat{T}^{-1}\hat{Q}^{-1}[1\hat{/}m]_{\text{ellipsoid}}\hat{Q}\hat{T}$ (Fig. 1b) from the coordinate system (K_X, K_Y, K_Z) of each ellipsoid to the system K_X'', K_Y'', K_Z''.[13]

The transformation from (K_X, K_Y, K_Z) to (K_X', K_Y', K_Z') is performed with the matrix $\hat{Q} = \begin{bmatrix} c & 0 & -s \\ 0 & 1 & 0 \\ s & 0 & c \end{bmatrix}$, and from K_X, K_Y, K_Z to (K_X'', K_Y'', K_Z'') with $\hat{T} = \begin{bmatrix} a_v & b_v & 0 \\ -b_v & a_v & 0 \\ 0 & 0 & 1 \end{bmatrix}$, where $c = \cos(\varphi)$, $s = \sin(\varphi)$, $a_v = \cos(\phi_v)$, $b_v = \sin(\phi_v)$, and $\phi_v = v(\pi/3)$ with $v = \{1,2,\ldots,6\}$.

After summation of the six valleys, the elements $[1/m]_{xx} = [1/m]_{yy} = 3(c^2/m_1 + 1/m_2 + s^2/m_3)$ and $[1/m]_{zz} = 6(s^2/m_1 + c^2/m_3)$ are the inverse of the inertial effective mass along the axis **a** (along K_X'' and K_Y'') and along **c** (along K_Z''), respectively.

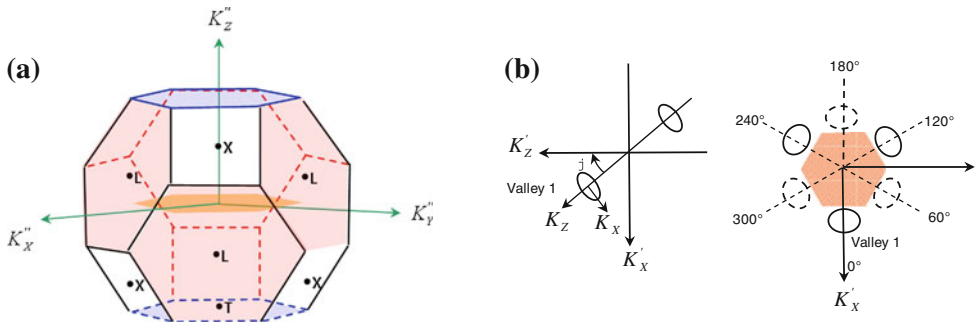

Fig. 1. (a) First Brillouin zone of Bi_2Te_3, Sb_2Te_3, and $75\%Sb_2Te_3$-$25\%Bi_2Te_3$. (b) Intermediary coordinate systems used to express the tensor $[1/m]$ in the coordinate system (K_X'', K_Y'', K_Z'').

Table I. Density-of-states effective mass of a single valley (m^*), density-of-state effective mass for the six valleys (m_d), inertial effective mass ($m_{\perp c}$) along the axis a, and ($m_{\| c}$) along the axis c, calculated from the longitudinal (m_3) and two transverse effective masses (m_1, m_2) of the $N_v = 6$ ellipsoids describing the constant-energy surfaces in k-space

	n-Bi_2Te_3	p-Bi_2Te_3	Sb_2Te_3	75%Sb_2Te_3-25%Bi_2Te_3
$m_1[m_0]$	0.081	0.196	0.127	0.144
$m_2[m_0]$	0.021	0.064	0.084	0.079
$m_3[m_0]$	0.320	0.730	1.24	1.6
$m^* = (m_1 m_2 m_3)^{1/3}$	0.081	0.209	0.236	0.263
$m_d = N_V^{2/3}(m_1 m_2 m_3)^{1/3}$	0.269	0.690	0.780	0.869
θ [°]	33.0	39.6	52.4	49.2
$m_{I\| c} = 6/(1/m)_{ZZ} = 1/(s^2/m_1 + c^2/m_3)$	0.104	0.278	0.290	0.301
$m_{I\perp c} = 6/(1/m)_{XX} = 2/(c^2/m_1 + 1/m_2 + s^2/m_3)$	0.037	0.108	0.116	0.118
$m^{*3/2}/m_{I\| c}$	0.221	0.343	0.395	0.448
$m^{*3/2}/m_{I\perp c}$	0.623	0.884	0.988	1.143
$m_{I\perp c}/m_{I\| c}$	2.81	2.57	2.50	2.55

Effective masses are normalized to the free electron mass.

The inertial and density-of-states effective masses, calculated with the data for m_1, m_2, and m_3 found in the literature for Bi_2Te_3, Sb_2Te_3, and the solid solution 75%Sb_2Te_3-25%Bi_2Te_3, are given in Table I. It is remarkable that m_1, m_2, $m_{\perp c}$, $m_{\| c}$, and $\theta = \pi/2 - \varphi$ for 75%Sb_2Te_3-25%Bi_2Te_3 are very well approximated by a Vegard-like law. However, m_3 for 75%Sb_2Te_3-25%Bi_2Te_3 is much higher than predicted by the Vegard law. In fact, the high value of m_3 partially explains the higher figure of merit of the solid solution compared with the pure compounds Bi_2Te_3 and Sb_2Te_3, as discussed below.

Boltzmann's Transport Equation

By using Boltzmann's equation and Gibbs' fundamental equation for the internal energy, and assuming that there is just one type of carrier and a parabolic energy dispersion, the electrical conductivity σ, the Seebeck coefficient α, and the electronic part of the thermal conductivity κ_e are given by

$$\sigma = \frac{e^2}{3\pi^2}\left(\lambda + \frac{3}{2}\right)\tau_0 \frac{2^{3/2}(k_B T)^{3/2+\lambda}}{\hbar^3}\frac{N_V m^{*3/2}}{m_I} F_{1/2+\lambda}(\zeta^*), \tag{1}$$

$$\alpha = \mp\frac{k_B}{e}\left[\zeta^* - \frac{(5/2+\lambda)F_{3/2+\lambda}(\zeta^*)}{(3/2+\lambda)F_{1/2+\lambda}(\zeta^*)}\right], \tag{2}$$

$$\kappa_e = \frac{\tau_0}{6\pi^2}\frac{2^{5/2}(k_B T)^{5/2+\lambda}}{\hbar^3}\frac{N_V m^{*3/2}}{m_I}k_B \times\left[\left(\frac{7}{2}+\lambda\right)F_{5/2+\lambda}(\zeta^*) - \frac{(5/2+\lambda)^2 F_{3/2+\lambda}^2(\zeta^*)}{(3/2+\lambda)F_{1/2+\lambda}(\zeta^*)}\right], \tag{3}$$

where $F_r(\zeta^*) = \int_0^\infty \frac{x^r}{1+e^{x-\zeta^*}}dx$ is the Fermi–Dirac integral and ζ^* is the normalized Fermi level ($\varepsilon_F/k_B T$). Supposing that the electrons are scattered by acoustic phonons, the relaxation time is $\tau(E) = \tau_0 E^\lambda$, where $\lambda = -½$ and E is the energy of an electron. The carrier concentration n, the density-of-states effective mass of a single valley, and the Fermi level are related by

$$n - \frac{N_V}{2\pi^2}\left(2m^* k_B T/\hbar^2\right)^{3/2} F_{1/2}(\zeta^*) = 0. \tag{4}$$

For a given carrier concentration, the Fermi level will be lower when the effective mass is higher, resulting in a higher Seebeck coefficient. The figure of merit $\sigma\alpha^2/\kappa$ increases with increasing quality factor

$$B = \frac{1}{3\pi^2}\frac{2^{3/2}}{\hbar^3}(k_B T)^{5/2+\lambda}\tau_0 N_V \frac{m^{*3/2}}{m_I}k_B\frac{1}{\kappa_L}, \tag{5}$$

where m_I is the inertial effective mass and N_V is the number of valleys. The thermal conductivity κ is the sum of electronic (κ_e) and lattice (κ_L) contributions.

CALCULATION METHODS FOR POLYCRYSTAL PROPERTIES

Invariance Method

The method described here is based on an averaging of the local tensor of the inverse effective mass over the whole sample volume. Local tensors can be calculated in each grain from the tensor of the inverse effective mass of the single crystal by matrix rotation, similar to the calculation of inertial effective masses in the coordinate system of the first Brillouin zone. The method is expected to yield reasonable estimates if the current density

varies only weakly with position in the sample. Furthermore, the boundary resistance between the grains should be negligible.

Since the trace remains invariant when a tensor is expressed in another coordinate system, the trace of the tensor of the inverse effective mass expressed in the coordinate system of the single crystal and the trace of the average of the local tensors over the whole sample in the polycrystal are identical:

$$\mathrm{tr}\langle[1/m]\rangle_{\mathrm{poly}} = \mathrm{tr}[1/m]_{\mathrm{single}}. \tag{6}$$

Since transport properties in directions perpendicular to the pressing direction are all equal, the tensor is diagonal, and

$$1/m_{\mathrm{I}\parallel\mathrm{pressing}_{\mathrm{poly}}} + 2/m_{\mathrm{I}\perp\mathrm{pressing}_{\mathrm{poly}}} = 1/m_{\mathrm{I}\parallel\mathbf{c}_{\mathrm{single}}} + 2/m_{\mathrm{I}\perp\mathbf{c}_{\mathrm{single}}}.$$

Analogous to the tensor of the inverse effective mass, the electrical conductivity and the lattice thermal conductivity obey the following relations:

$$\sigma_{\parallel\mathbf{c}_{\mathrm{poly}}} = \sigma_{\parallel\mathbf{c}_{\mathrm{single}}} + 2\sigma_{\perp\mathbf{c}_{\mathrm{single}}} - 2\sigma_{\perp\mathbf{c}_{\mathrm{poly}}}, \tag{7}$$

$$\kappa_{\mathrm{L}\perp\mathbf{c}_{\mathrm{poly}}} = \left(\kappa_{\mathrm{L}\parallel\mathbf{c}_{\mathrm{single}}} + 2\kappa_{\mathrm{L}\perp\mathbf{c}_{\mathrm{single}}} - \kappa_{\mathrm{L}\parallel\mathbf{c}_{\mathrm{poly}}}\right)/2. \tag{8}$$

Since sintered materials such as Bi_2Te_3 are usually textured, the distinct pressing direction is chosen as the c-axis of the polycrystal, denoted by $\parallel \mathbf{c}_{\mathrm{poly}}$ in the above formulas.

Obviously $\sigma_{\parallel\mathbf{c}_{\mathrm{poly}}}$ must be smaller than the highest value of the electrical conductivity in the single crystal $\sigma_{\perp\mathbf{c}_{\mathrm{single}}}$. Consequently, $\sigma_{\perp\mathbf{c}_{\mathrm{single}}} > \sigma_{\parallel\mathbf{c}_{\mathrm{poly}}} = \sigma_{\parallel\mathbf{c}_{\mathrm{single}}} + 2\sigma_{\perp\mathbf{c}_{\mathrm{single}}} - 2\sigma_{\perp\mathbf{c}_{\mathrm{poly}}}$, and after rearrangement it can be found that

$$\sigma_{\perp\mathbf{c}_{\mathrm{poly}}} > (\sigma_{\parallel\mathbf{c}_{\mathrm{single}}} + \sigma_{\perp\mathbf{c}_{\mathrm{single}}})/2. \tag{9}$$

Thus, the electrical conductivity of a sintered material should be larger than $(\sigma_{\parallel\mathbf{c}_{\mathrm{single}}} + \sigma_{\perp\mathbf{c}_{\mathrm{single}}})/2$ and smaller than $\sigma_{\perp\mathbf{c}_{\mathrm{poly}}}$, where $\sigma_{\parallel\mathbf{c}_{\mathrm{single}}}$ and $\sigma_{\perp\mathbf{c}_{\mathrm{single}}}$ are calculated at the same carrier concentration as in the polycrystal. When the grain orientation distribution is isotropic, the electrical conductivity of the polycrystal is approximated by

$$\sigma_{\mathrm{isopoly}} = \left(\sigma_{\parallel\mathbf{c}_{\mathrm{single}}} + 2\sigma_{\perp\mathbf{c}_{\mathrm{single}}}\right)/3. \tag{10}$$

RVE Method

Since the hypotheses made to derive the formulae (8–10) are never truly fulfilled, the RVE method has been used for determining the polycrystal properties. This method allows for the calculation of the macroscopic or effective properties of the polycrystalline material, knowing single-crystal data and the material texture. In view of the special preparation procedure of the thermoelectric material, the resulting polycrystal is supposed to show macroscopic transversal anisotropy with respect to the pressing direction. The microscopic properties of the grains with hexagonal crystal symmetry also exhibit transversal anisotropy (cf. Tables II and III). Because of the macroscopic transversal anisotropy it is thus sufficient to know the frequency distribution of the c-axis orientation of the grains with respect to the pressing direction to determine the effective material properties of the polycrystal. The frequency distribution of the c-axis orientation can be derived from results of electron backscattering diffraction (EBSD) analysis performed on a sample cross-section perpendicular to the pressing direction.[14,15] The orientation distribution is fitted by the formula $p(\cos\theta) = a_1\,(a_2 + (\cos\theta)^{a_3})$, where θ denotes the angle between the pressing direction

Table II. Transport properties of Bi_2Te_3, Sb_2Te_3, and 75%Sb_2Te_3-25%Bi_2Te_3 single crystals, measured along the *a*-axis (taken from Ref. 17)

	Bi_2Te_3	Sb_2Te_3	75%Sb_2Te_3-25%Bi_2Te_3
$\sigma_{\perp\mathbf{c}}$ [Ω^{-1} cm^{-1}]	1000	8196	1005
$\alpha_{\perp\mathbf{c}}$ [μV K^{-1}]	−240	63	194
$\kappa_{\perp\mathbf{c}}$ [W m^{-1} K^{-1}]	2.2	7.47	1.26
$ZT_{\perp\mathbf{c}}$	0.78	0.13	0.90
$\sigma_{\parallel\mathbf{c}}$ [Ω^{-1} cm^{-1}]	185	3095	386
$\alpha_{\parallel\mathbf{c}}$ [μV K^{-1}]	$(-240 = \alpha_{\perp\mathbf{c}})$	92	$(194 = \alpha_{\perp\mathbf{c}})$
$\kappa_{\parallel\mathbf{c}}$ [W m^{-1} K^{-1}]	1.0	1.63	~0.55
$ZT_{\parallel\mathbf{c}}$	0.31	0.48	0.79
$\sigma_{\perp\mathbf{c}}/\sigma_{\parallel\mathbf{c}}$	5.4	2.6	2.6
$\kappa_{\perp\mathbf{c}}/\kappa_{\parallel\mathbf{c}}$	2.2	4.6	1.59
$ZT_{\perp\mathbf{c}}/ZT_{\parallel\mathbf{c}}$	2.5	0.27	1.13

The carrier concentrations for Bi_2Te_3, Sb_2Te_3, and 75%Sb_2Te_3-25%Bi_2Te_3 are 2.3×10^{19} cm^{-3}, 2.1×10^{20} cm^{-3} and 4.8×10^{19} cm^{-3}, respectively.

Table III. Calculated transport properties along the *a*-axis of Bi_2Te_3, Sb_2Te_3, and 75%Sb_2Te_3-25%Bi_2Te_3 single crystals

	Bi_2Te_3	Sb_2Te_3	75%Sb_2Te_3-25%Bi_2Te_3
$\sigma_{\perp \mathbf{c}}$ $[\Omega^{-1}\ \mathrm{cm}^{-1}]$	1000 (=exp)	8196 (=exp)	1005 (=exp)
$\alpha_{\perp \mathbf{c}}$ $[\mu \mathrm{V\ K}^{-1}]$	−240	64	194
$\kappa_{\perp \mathbf{c}}$ $[\mathrm{W\ m}^{-1}\ \mathrm{K}^{-1}]$	2.2	6.25	1.26
$\kappa_{\mathrm{L}\perp \mathbf{c}}$ $[\mathrm{W\ m}^{-1}\ \mathrm{K}^{-1}]$	1.73	2.25	0.77
$\kappa_{e\perp \mathbf{c}}$ $[\mathrm{W\ m}^{-1}\ \mathrm{K}^{-1}]$	0.47	5.25	0.49
$ZT_{\perp \mathbf{c}}$	1.01	0.13	0.89
$\sigma_{\parallel \mathbf{c}}$ $[\Omega^{-1}\ \mathrm{cm}^{-1}]$	315	3286	394.7
$\alpha_{\parallel \mathbf{c}}$ $[\mu \mathrm{V\ K}^{-1}]$	−240(=$\alpha_{\perp \mathbf{c}}$)	(= $\alpha_{\perp \mathbf{c}}$)	194(= $\alpha_{\perp \mathbf{c}}$)
$\kappa_{\parallel \mathbf{c}}$ $[\mathrm{W\ m}^{-1}\ \mathrm{K}^{-1}]$	0.79	2.1	0.89
$\kappa_{\mathrm{L}\parallel \mathbf{c}}$ $[\mathrm{W\ m}^{-1}\ \mathrm{K}^{-1}]$	0.64	0	0.36
$\kappa_{\mathrm{e}\parallel \mathbf{c}}$ $[\mathrm{W\ m}^{-1}\ \mathrm{K}^{-1}]$	0.17	2.10	0.19
$ZT_{\parallel \mathbf{c}}$	0.69	0.19	0.80
$\sigma_{\perp \mathbf{c}}/\sigma_{\parallel \mathbf{c}}$	3.17	2.49	2.55
$\kappa_{\mathrm{L}\perp \mathbf{c}}/\kappa_{\mathrm{L}\parallel \mathbf{c}}$	2.7	–	3.5
$\kappa_{\perp \mathbf{c}}/\lambda_{\parallel \mathbf{c}}$	2.78	2.97	1.59
$ZT_{\perp \mathbf{c}}/ZT_{\parallel \mathbf{c}}$	1.46	0.68	1.11

The normalized Fermi level ζ^* and the prefactor τ_0 are used as adjustment variables to match the Seebeck coefficient and the electrical conductivity to the corresponding measured values along the *a*-axis. The normalized Fermi level was set to −0.55 for Bi_2Te_3, 4.3 for Sb_2Te_3, and 0.18 for 75%Sb_2Te_3-25%Bi_2Te_3.

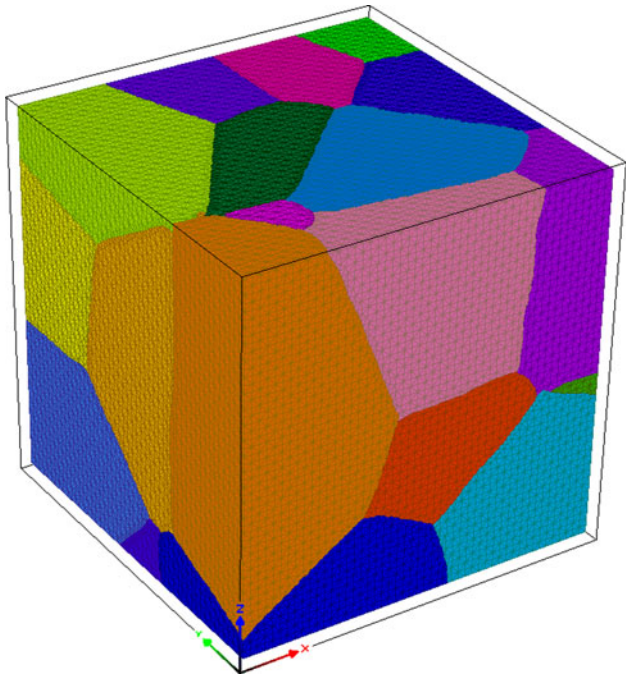

Fig. 2. View of the artificially generated polycrystal with 27 grains. The finite-element mesh was constructed by using the software package Simpleware.

and the *c*-axis of a grain, and the parameters a_1, a_2, and a_3 are chosen to match the measured frequency distribution.

In order to calculate the effective material properties of the sintered polycrystal within the framework of the RVE method, an artificial polycrystal with 27 grains was generated (Fig. 2). The crystal orientation of each grain was chosen randomly according to the grain orientation distribution of the textured material. Then the effective properties of this polycrystal with a particular realization of grain orientations were calculated by means of the finite-element software COMSOL Multiphysics.[16] The calculations were repeated for further orientation realizations. Because of the finite size of our polycrystal model with 27 grains, the calculated effective properties show a certain scatter for different grain orientation realizations. The effective material properties presented below represent averages over 100 generated orientation realizations of the shown polycrystal model.

Effective Conductivities

The calculation of the effective electric conductivity is mathematically equivalent to that for the thermal conductivity. We thus present only the case of thermal conductivity. The cubical polycrystal model is aligned parallel to the axes of a (x, y, z) coordinate system with the pressing direction parallel to the z-axis. To determine the effective thermal conductivity in the z-direction, $\kappa_{\mathrm{eff},zz}$, we apply a temperature difference $T_2 - T_1$ between the bottom and top face of the polycrystal and calculate

the heat flux in the sample by solving the stationary heat conduction equation

$$\nabla_i \kappa_{ik}(\mathbf{r}) \nabla_k T(\mathbf{r}) = \mathbf{0} \tag{11}$$

(Einstein sum convention), where $\kappa_{ik}(\mathbf{r})$ is the tensor of thermal conductivity in the grains, which varies from grain to grain due to grain orientation changes. The other side-faces of the polycrystal are insulated. The effective conductivity in the z-direction results then from Fourier's law as

$$\kappa_{\text{eff},zz} = \frac{d_z}{T_2 - T_1}\langle j_{zz}\rangle, \tag{12}$$

where $\langle j_{zz}\rangle$ is the area average of the heat flux over a cross-section of the sample perpendicular to the z-axis, and d_z is the side length of the considered polycrystal cube. The effective thermal conductivity in the transverse direction is obtained analogously by applying a temperature difference in, for example, the x-direction.

Effective Seebeck Coefficient

For determining the effective Seebeck coefficient, $\alpha_{\text{eff},ik}$, two fields have to be considered, namely the temperature T and the electric potential V. They obey the coupled equations[16,17]

$$\nabla_i \sigma_{ik}(\nabla_k V + \alpha_{kl}\nabla_l T) = 0, \tag{13}$$

$$\begin{aligned} &-\nabla_i \kappa_{ik}\nabla_k T - \nabla_i T \alpha_{ik}\sigma_{kl}(\nabla_l V + \alpha_{lm}\nabla_m T) \\ &\quad = (\nabla_i V)\,\sigma_{ik}(\nabla_k V + \alpha_{kl}\nabla_l T), \end{aligned} \tag{14}$$

where the thermal and electric conductivities, κ_{ik} and σ_{ik}, as well as the Seebeck coefficient α_{ik}, change again from grain to grain. To determine, for example, the effective Seebeck coefficient in the z-direction, a temperature difference $T_2 - T_1$ is applied between the bottom and top face of the polycrystal. For the potential, a voltage V_1 is given only on the bottom face. The temperature and potential fields are calculated under the condition of vanishing electric current density on the top and bottom face. The other side-faces are thermally and electrically insulated. The effective Seebeck coefficient parallel to the pressing direction is then determined via the formula

$$\alpha_{\text{eff},zz} = \frac{\langle V_2\rangle - V_1}{T_2 - T_1}, \tag{15}$$

where $\langle V_2\rangle$ is the area average of the potential on the top face. The transverse effective Seebeck coefficient is obtained by analogous calculations in the transverse direction.

RESULTS

Transport Properties of Single Crystals

Generally accepted data of measured transport properties[18] of Bi_2Te_3, Sb_2Te_3, and 75%Sb_2Te_3-25%Bi_2Te_3 are summarized in Table II. These data can be compared with results in Table III obtained within the one-parabolic-band model. Since the parameter τ_0 is unknown and the Seebeck coefficient, calculated with Eqs. 2 and 4, is systematically too low compared with the experimental value, the parabolic band model had to be calibrated. τ_0 was assumed isotropic and was calculated by setting $\sigma_{\perp\mathbf{c}}$ equal to the experimental value. Similarly, instead of using Eq. 2, ζ^* had to be adjusted to match the experimental value of $\alpha_{\perp\mathbf{c}}$. κ_L was also adjusted to match the experimental value of κ.

Despite its simplicity, the model accurately predicts the anisotropy of the electrical conductivity of 25%Bi_2Te_3-75%Sb_2Te_3. The agreement between experiment and model is also very good for the anisotropy of the electrical conductivity of Sb_2Te_3. Nevertheless a one-band model cannot explain the anisotropy of the Seebeck coefficient measured on Sb_2Te_3, therefore more bands should be taken into account.[17] The predicted anisotropy of the electrical conductivity of n-Bi_2Te_3 was less than the measured one. At present, it is unclear whether this discrepancy is related to insufficient accuracy of the theoretical estimate or to experimental errors. However, a nonparabolic band approximation would probably lead to better agreement between theory and experiment.

The calculated lattice thermal conductivity and its anisotropy are in good agreement with both experimental data and ab initio calculation.[8] The lattice thermal conductivity along the c-axis of the solid solution 25%Bi_2Te_3-75%Sb_2Te_3 (0.36 W m^{-1} K^{-1}) was found to be much lower than for the pure compound Bi_2Te_3 (0.64 W m^{-1} K^{-1}). The lattice thermal conductivity of the Bi_2Te_3-Sb_2Te_3 solution is larger than in a Bi_2Te_3-Sb_2Te_3 superlattice[19] (lattice thermal conductivity 0.22 W m^{-1} K^{-1}). It is noteworthy that the ratios $m^{*3/2}/m_{\text{I}\perp\mathbf{c}}$ and $m^{*3/2}/m_{\text{I}\parallel\mathbf{c}}$ are significantly larger for 25%Bi_2Te_3-75%Sb_2Te_3 than for p-Bi_2Te_3 (Table I), and a larger quality factor (Eq. 5) is expected for the solid solution than for the compound. Finally, the slightly larger density-of-states effective mass of the solid solution, compared with p-Bi_2Te_3 and Sb_2Te_3, favors a lower Fermi level and consequently a larger Seebeck coefficient.

Invariance Method

The invariance method has been tested on sintered 25%Bi_2Te_3-75%Sb_2Te_3 samples, whose transport properties have been measured parallel and perpendicular to the pressing direction (Table IV). A detailed description of the measurement system used is given in Ref. 20. It has been extended for measurements up to 600°C. Sample preparation is discussed elsewhere.[15] The present numerical model was calibrated by using the Seebeck coefficient and the electrical conductivity measured along the a-axis on a 25%Bi_2Te_3-75%Sb_2Te_3 single crystal in order to find the value of τ_0. After that, the Fermi

Table IV. Comparison between measured transport properties on standard spark plasma sintered materials (Standard-SPS) and values calculated by the invariance method (Fermi level set to 0.18)

	Model of the Single Crystal at ζ^*_{poly}		Standard-SPS (Experiment)		Standard-SPS (Invariance Method)	
75%Sb_2Te_3-25%Bi_2Te_3	**$\perp$c**	**$\parallel$c**	**$\perp$ Pressing Direction**	**$\parallel$ Pressing Direction**	**$\perp$ Pressing Direction**	**$\parallel$ Pressing Direction**
σ (Ω^{-1} cm^{-1})	1012	397.4	837	607	837 (exp)	733
α (μV K^{-1})	194	194	175	193	193 (exp)	193 (exp)
λ (W m^{-1} K^{-1})	1.26	0.55	1.28	0.88	1.13	0.88 (exp)
λ_e (W m^{-1} K^{-1})	0.49	0.19	0.41	0.30	0.41	0.43
λ_L (W m^{-1} K^{-1})	0.77	0.36	0.87	0.58	0.72	0.45
ZT (T = 300 K)	0.89	0.80	0.60	0.77	0.82	0.93

Table V. Calculated effective transport properties for an Sb_2Te_3 polycrystal with and without texture, in comparison with the transport properties of the single crystal (orientation distribution parameters $a_1 = 4.34$, $a_2 = 0.094$, $a_3 = 6.34$)

	Single Crystal			Textured Polycrystal	
	$\perp$c	**$\parallel$c**	**Isotropic Polycrystal**	**$\perp$ Pressing Direction**	**$\parallel$ Pressing Direction**
σ (Ω^{-1} cm^{-1})	8196	3095	6156	6922	4800
α (μV K^{-1})	63.0	92.0	71.9	68.4	79.2
λ (W m^{-1} K^{-1})	7.47	1.63	4.95	5.86	3.41
ZT (T = 300 K)	0.13	0.48	0.19	0.16	0.26

level ζ^* was adjusted to match the value of the Seebeck coefficient measured on the polycrystalline material, which in the model is supposed to be isotropic. The Fermi level then takes the value ζ^*_{poly}. The electrical conductivity of the single crystal was calculated along **a** and **c** with the Fermi level ζ^*_{poly} and used in Eq. 7 to calculate the electrical conductivity of the polycrystal parallel to the pressing direction, where the electrical conductivity perpendicular to the pressing direction was known from measurement. The electronic part of the thermal conductivity was then calculated parallel and perpendicular to the pressing direction. The lattice thermal conductivity of the polycrystal parallel to the pressing direction can be deduced from the measured total thermal conductivity in this direction. The lattice thermal conductivity of the polycrystal perpendicular to the pressing direction was calculated using Eq. 8. Although the results of the invariance method seem to agree quite well with experimental data, we stress that inconsistent results can be obtained with inappropriate single-crystal data. Choosing arbitrarily, for the sake of demonstration, a single-crystal Seebeck coefficient of 175 μV K^{-1} instead of 193 μV K^{-1}, the calculated electrical conductivity would have been larger (1302 Ω^{-1} cm^{-1}) parallel to the pressing direction than along the a-axis of the single crystal (1244 Ω^{-1} cm^{-1}). Furthermore, according to the invariance method (Eq. 9), the electrical conductivity perpendicular to the pressing direction cannot be smaller than $(\sigma_{\parallel \mathbf{c}_{single}} + \sigma_{\perp \mathbf{c}_{single}})/2$. Nevertheless, values lower than the last expression could be measured in cases where boundary resistances between the grains are important, for example, in very fine-grained materials. The invariance method does not include boundary resistances and is therefore not suited for describing nanocrystalline materials.

RVE Method

The calculated effective material properties of polycrystalline Sb_2Te_3 for both isotropic and anisotropic grain orientation distribution are presented in Table V together with the single-crystal data. The considered example texture exhibits preferred c-axis grain orientation near the pressing direction. For the isotropic orientation distribution, the RVE results are in good agreement with analytical estimates ($\lambda_{eff} = 4.96\,\mathrm{W\,m^{-1}\,K^{-1}}$, $\lambda_{eff} = 6160\,\Omega^{-1}\,\mathrm{cm^{-1}}$).[21] It has to be emphasized that the present calculation of effective properties is based on a continuum theory which does not take into

account thermal boundary resistance between the grains. Thus, differences between the present theoretical values for the effective properties and the experimentally measured values should reveal the impact of grain boundaries.

CONCLUSIONS

The presented method for calculation of the inertial effective masses has proven sufficient to understand the anisotropy of the electrical conductivity of Sb_2Te_3 single crystal and its solid solution with Bi_2Te_3. However, the use of a one-band model failed to explain the anisotropy of the Seebeck coefficient of Sb_2Te_3, and the anisotropy of the electrical conductivity predicted for n-Bi_2Te_3 is less than the experimental one. Despite the success of the model in improving understanding of the better electrical and thermal properties of solid solutions, it is evident that more than one band and nonparabolicity must be taken into account. For calculating the effective material properties of a polycrystal, the representative volume element method is an appropriate tool if detailed information on the microstructure is available. For more accurate quantitative description of the transport properties of fine-grained materials, interfacial thermal resistance and possibly also electrical resistance of grain boundaries should be included in future analysis.

ACKNOWLEDGEMENTS

The authors thank Marian Böhling, who worked at the Institut für Werkstoffwissenschaft, Technische Universität Dresden, for performing the EBSD analysis. This work was supported by the German Federal Ministry of Education and Research (BMBF) within the joint project VEKTRA.

REFERENCES

1. H.J. Goldsmidt and M. Situmorang, *Proceedings of the 8th International Conference on Thermoelectrics*, *Nancy, France* (1989), p. 1.
2. J. Jiang, L. Chen, S. Bai, Q. Yao, and Q. Wang, *Mater. Sci. Eng. B* 117, 334 (2005).
3. L. Chaput, *Calculation of the Transport Properties of Thermoelectric Materials* (France: PhD Polytechnic Institute of Lorraine, 2006).
4. T.J. Scheidemantel, C. Ambrosch-Draxl, T. Thonhauser, J.V. Badding, and J.O. Sofol, *Phys. Rev. B* 68, 125210 (2003).
5. S.K. Mishra, S. Satpathy, and O. Jepsen, *J. Phys. Condens. Matter* 9, 461 (1997).
6. L. Chaput, P. Pécheur, and H. Scherrer, *Phys. Rev. B* 75, 045116 (2007).
7. C. Herring and E. Vogt, *Phys. Rev*. 101, 944 (1956).
8. B.-L. Huang and M. Kaviany, *Phys. Rev. B* 77, 125209 (2008).
9. Landolt-Börnstein, *Group III Condensed Matter*, ed. H. Fischer (Berlin, Heidelberg: Springer, 1988), ISSN 1615-1925.
10. M. Stordeur, M. Stölzer, H. Sobotta, and V. Riedle, *Phys. Stat. Solidi (b)* 150, 165 (1988).
11. J.R. Drabble and R. Wolfe, *Proc. Phys. Soc. B* 69, 1101 (1956).
12. A. Jacquot, *Proceedings of the European Conference on Thermoelectrics*, *Paris, France* (2008), p. 1.
13. J.H. Dennis, *Technical Report 377* (Cambridge: Research Laboratory of Electronics, Massachusetts Institute of Technology, January 15, 1961), 52 p.
14. V. Randle and O. Engler, *Texture Analysis—Macrotexture, Microtexture & Orientation Mapping* (Boca Raton, FL: CRC, 2009), 480 p.
15. D.G. Ebling, A. Jacquot, J. König, H. Böttner, J. Schmidt, and P. Spies, *Proceedings of the 26th International Conference on Thermoelectrics*, *Korea, O-D-6* (2007).
16. D.G. Ebling, M. Jaegle, M. Bartel, A. Jacquot, and H. Böttner, *J. Electron. Mater.* 38, 1456 (2009). doi: 10.1007/s11664-009-0825-0.
17. E.E. Antonova and D.C. Looman, *Proceedings of the 24th International Conference on Thermoelectrics,* Clemson, USA (2005), p. 215.
18. H. Scherrer and S. Scherrer, *Handbook of Thermoelectrics* (Boca Raton, FL: CRC, 1995), Chap. 19.
19. R. Venkatasubramanian, E. Siivola, T. Colpitts, and B. O'Quinn, *Nature* 413, 597 (2001).
20. A. Jacquot, J. König, and H. Böttner, *Proceedings of the 25th International Conference on Thermoelectrics*, Vienna, Austria (2006), p. 184.
21. G.W. Milton, *The Theory of Composites* (Cambridge: Cambridge University Press, 2002), Chap. 10.